(12)

GALVANIC CORROSION OF ALUMINUM-MATRIX COMPOSITES

by

L.H. Hihara and R.M. Latanision

Technical Report No. 2
to
Office of Naval Research
Grant No. N00014-89-J-1588

The H.H. Uhlig Corrosion Laboratory
Department of Materials Science and Engineering
Massachusetts Institute of Technology
Cambridge, Massachusetts 02139

February 1991

SECURITY CLASSIFICATION OF THIS PAGE

REPORT DOCUMENTATION PAGE

Form Approved
OMB No 0704-0188

1a REPORT SECURITY CLASSIFICATION Unclassified	1b RESTRICTIVE MARKINGS
2a SECURITY CLASSIFICATION AUTHORITY	3 DISTRIBUTION / AVAILABILITY OF REPORT
2b DECLASSIFICATION / DOWNGRADING SCHEDULE	
4 PERFORMING ORGANIZATION REPORT NUMBER(S)	5 MONITORING ORGANIZATION REPORT NUMBER(S)
6a NAME OF PERFORMING ORGANIZATION Massachusetts Institute of Technology 6b OFFICE SYMBOL (If applicable)	7a NAME OF MONITORING ORGANIZATION Office of Naval Research
6c ADDRESS (City, State, and ZIP Code) Room 8-202, 77 Massachusetts Avenue Cambridge, MA 02139	7b ADDRESS (City, State, and ZIP Code) 800 N. Quincy Street Arlington, VA 22217-5000
8a NAME OF FUNDING / SPONSORING ORGANIZATION Office of Naval Research 8b OFFICE SYMBOL (If applicable)	9 PROCUREMENT INSTRUMENT IDENTIFICATION NUMBER
8c ADDRESS (City, State, and ZIP Code) Arlington, VA 22217-5000	10 SOURCE OF FUNDING NUMBERS PROGRAM ELEMENT NO: 89-J-1588 / PROJECT NO: cor5523-02 / TASK NO / WORK UNIT ACCESSION NO

11 TITLE (Include Security Classification)
Galvanic Corrosion of Aluminum-Matrix Composites

12 PERSONAL AUTHOR(S)
L.H. Hihara and R.M. Latanision

13a TYPE OF REPORT	13b TIME COVERED	14 DATE OF REPORT (Year, Month, Day)	15 PAGE COUNT
Technical Report	FROM 1 Mar90 TO 31Dec90	February 1991	33

16 SUPPLEMENTARY NOTATION

17 COSATI CODES			18 SUBJECT TERMS (Continue on reverse if necessary and identify by block number)
FIELD	GROUP	SUB-GROUP	Corrosion, Aluminum-Matrix Composites

19 ABSTRACT (Continue on reverse if necessary and identify by block number)

Galvanic-corrosion rates of Al-matrix composites were high in aerated chloride-containing solutions. Oxygen reduction was found to be the primary cathodic reaction. Aluminum corroded by pitting. The type of noble constituent (i.e., graphite, SiC, or TiB_2) also affected galvanic-corrosion rates. For example, results indicated that the galvanic-corrosion rate of Al should be about 30 times greater when coupled to graphite than when coupled to SiC or TiB_2. In dearated solutions, galvanic corrosion was negligible even if chlorides were present. The galvanic-corrosion rates were determined using the zero-resistance ammeter technique and from potentiodynamic polarization diagrams of ultrapure Al, 6061-T6 Al, graphite fiber, SiC, TiB_2, and a commercial graphite fiber/6061-T6 Al metal-matrix composite.

20 DISTRIBUTION / AVAILABILITY OF ABSTRACT	21 ABSTRACT SECURITY CLASSIFICATION
☒ UNCLASSIFIED/UNLIMITED ☐ SAME AS RPT ☐ DTIC USERS	Unrestricted
22a NAME OF RESPONSIBLE INDIVIDUAL A.J. Sedriks	22b TELEPHONE (Include Area Code) (202) 696-4401 22c OFFICE SYMBOL 1131 M

DD Form 1473, JUN 86 *Previous editions are obsolete* SECURITY CLASSIFICATION OF THIS PAGE

S/N 0102-LF-014-6603

Galvanic Corrosion of Aluminum-Matrix Composites

L.H. Hihara[1] and R.M. Latanision[2]

[1]Department of Mechanical Engineering
University of Hawaii at Manoa
Honolulu, Hawaii 96822

[2]The H.H. Uhlig Corrosion Laboratory
Department of Materials Science and Engineering
Massachusetts Institute of Technology
Cambridge, MA 02139

Abstract

Galvanic-corrosion rates of Al-matrix composites were high in aerated chloride-containing solutions. Oxygen reduction was found to be the primary cathodic reaction. Aluminum corroded by pitting. The type of noble constituent (i.e., graphite, SiC, or TiB_2) also affected galvanic-corrosion rates. For example, results indicated that the galvanic-corrosion rate of Al should be about 30 times greater when coupled to graphite than when coupled to SiC or TiB_2. In deaerated solutions, galvanic corrosion was negligible even if chlorides were present. The galvanic-corrosion rates were determined using the zero-resistance ammeter technique and from potentiodynamic polarization diagrams of ultrapure Al, 6061-T6 Al, graphite fiber, SiC, TiB_2, and a commercial graphite fiber/6061-T6 Al metal-matrix composite.

Introduction

Galvanic corrosion is a concern in Al-matrix composites because Al, which is an active metal, is coupled to noble

reinforcement constituents such as graphite and SiC. The difference between the reversible potentials E_{REV} (at 25°C, unit activities, except pH set to 7) of $O_2 + 4H^+ + 4e^- = 2H_2O$ (E_{REV} = 0.82 V_{SHE}) and $Al^{3+} + 3e^- = Al$ (E_{REV} = -1.66 V_{SHE}) is 2.48 V, and that between $2H^+ + 2e^- = H_2$ (E_{REV} = -0.41 V_{SHE}) and $Al^{3+} + 3e^- = Al$ is 1.25 V [1]. Therefore, a galvanic couple will form between Al and the reinforcement constituents, which are inert electrodes upon which O_2 and H^+ reduction may occur. Accordingly, some authors speculate that galvanic corrosion is responsible for the higher corrosion rates observed in graphite fiber/aluminum (G/Al) and SiC/Al metal-matrix composites (MMCs) in comparison to their monolithic matrix alloys [2-8]. The galvanic-corrosion rate, however, cannot be obtained from the thermodynamic data. Therefore, kinetic studies were performed in this investigation to obtain information on the galvanic-corrosion rates of G/Al and SiC/Al MMCs.

The effect of O_2 reduction, H^+ reduction, and Al passivity on galvanic-corrosion rates in chloride-free and chloride-containing solutions was investigated. Experiments were performed in neutral, deaerated and aerated 0.5 M Na_2SO_4 and 3.15 wt% NaCl solutions at 30°C. Polarization diagrams were generated for ultrapure Al of 99.999% metallic purity (m5N Al), 6061-T6 Al, high-modulus graphite (P100 G) fiber, SiC, TiB_2, and a commercial G/6061-T6 Al MMC. TiB_2 was included in this study because it is sometimes used as a fiber coating to enhance the wettability of graphite fibers in molten Al alloys. Galvanic-corrosion rates were estimated from the polarization diagrams using the mixed-electrode theory. In addition, the zero-resistance ammeter (ZRA) technique was used to measure galvanic-corrosion rates of couples consisting of P100 G fiber and 6061-T6 Al.

Galvanic corrosion was severe in aerated 3.15 wt% NaCl. Oxygen reduction on the surface of reinforcement constituents accelerated pitting of the Al matrix. The corrosion rate of 6061-T6 Al increased by about 80 times when coupled to P100 G fiber of equal area. The type of reinforcement constituent also affected the galvanic-corrosion rate. It was estimated that the galvanic-corrosion rate of m5N Al and 6061-T6 Al would be about 30 times greater when coupled to P100 G than when coupled to SiC or TiB_2. In deaerated 3.15 wt% NaCl, galvanic corrosion was negligible. Proton reduction played a minimal role in galvanic corrosion.

Materials

m5N Al and 6061-T6 Al Electrodes:

Planar m5N Al and 6061-T6 Al electrodes were fabricated by coating specimens with either an epoxy paint (AMERCOAT 90 RESIN, Ameron) or an epoxy adhesive (EPOXY-PATCH, The Dexter Corporation). Following the coating procedure, one side of the specimens was ground flat. This removed the epoxy from one surface and exposed a planar electrode face. Electrodes were fabricated with either a 0.0233 cm^2 or a 0.811 cm^2 surface area. Both types of electrodes were used in potentiodynamic polarization experiments. The 0.0233 cm^2 electrode was also used in galvanic-couple experiments, in which the 6061-T6 Al electrode was coupled to a P100 G electrode of equal surface area. The 0.0233 cm^2 size was governed by the size of the graphite electrode (discussed below).

Graphite Electrodes:

Planar graphite electrodes were fabricated from Thornel P100 fibers, which are unidirectional, continuous, about 10 μm in diameter, and pitch-based with an elastic modulus equal to

690 GPa. Fifteen tows of the fiber (about 2000 fibers/tow) were aligned unidirectionally and infiltrated with an epoxy resin (EPON 828 RESIN, Miller-Stephenson Chemical Co., Inc.). The resulting product, a graphite/epoxy composite rod, was made into electrodes by sectioning the rod perpendicular to the axis of the fibers. The total cross-sectional surface area of the graphite fibers was about 0.0233 cm^2.

SiC and TiB_2 Electrodes:

Planar electrodes were fabricated from bars of SiC and TiB_2 that were purchased from Ceradyne, Inc. The SiC and TiB_2 were hot-pressed to near theoretical densities (>98%) without sintering aids or binders. The sides of the specimens were coated with EPOXY-PATCH. A planar electrode face was exposed by grinding the epoxy from one surface.

Special precautions were taken to make the SiC electrodes due to the high electrical resistivity of SiC. The SiC bars were first cut into 9 x 9 mm-square wafers about 1 mm thick. Then, to make electrodes, the entire back side of the SiC wafers was silver painted to make electrical contact. This procedure was followed to ensure that the IR drop through the SiC wafer was uniform over the electrode face during polarization experiments. Note that the polarization diagrams in this document have been corrected for the IR drop. The resistance through the thickness of the SiC wafers was about 10^3 ohm.

G/6061-T6 Al MMC Electrodes:

G/6061 Al MMC precursor wires were produced by Material Concept, Inc. The wires consisted of a tow of Thornel P100 graphite fibers infiltrated with 6061 Al to a volume fraction of about 0.5. Six-ply plates were consolidated by DWA Composite Specialties, Inc. by diffusion bonding six layers of

precursor wires between surface 6061 Al foils. The G/6061 Al MMCs were heat treated to the T6 condition by solution-treating at 530°C for 50 min, water quenching, and artificially aging at 160°C for 18 h.

Planar electrodes were made from G/6061-T6 Al MMC six-ply plates. The surface foils of the six-ply plate were ground away prior to making electrodes. The specimens were coated with AMERCOAT 90 RESIN and then mounted in EPON 828 RESIN. Following the coating procedure, a planar electrode face was exposed by grinding away the epoxy from one surface. The graphite fibers were oriented perpendicular to the electrode face.

Aqueous Solutions:

Neutral 0.5 M Na_2SO_4 and 3.15 wt% NaCl solutions were prepared from 18 x 10^6 ohm-cm water, and analytical grade Na_2SO_4 (< 0.0002% Cl) and NaCl, respectively. The solutions were kept at 30 ± 0.1°C, and deaerated with pre-purified hydrogen or aerated with 19.5 to 23.5 % oxygen balanced with nitrogen. Gas pressure was 1 atm.

Instrumentation and Procedure

The surface of all planar electrodes was polished to a 0.05 μm finish with gamma alumina powder, kept wet, and rinsed with 18 x 10^6 ohm-cm water about 5 minutes prior to immersion in the aqueous solutions.

Potentiodynamic Polarization Experiments:

Potentiodynamic polarization experiments were conducted with either a Model 273 EG&G Princeton Applied Research (PAR) potentiostat/galvanostat or a Model 173 EG&G PAR potentiostat/galvanostat equipped with a Model 376 EG&G PAR

logarithmic current converter. When measuring currents in the nA range, the accuracy of the instruments were measured to be better than 10%.

In generating potentiodynamic polarization diagrams, the electrodes were allowed to stabilize at their corrosion potential E_{CORR} before subsequently polarizing at a rate of 0.1 mV/s. Three or more polarization curves were generated for each experimental condition. The logarithm of the current density (CD) was averaged and plotted as a function of potential to generate the polarization diagrams in this document. The standard deviation of log i was also calculated. Standard-deviation bars of log i, however, were omitted from polarization diagrams for clarity because numerous diagrams were plotted in the same figure. Consequently, the reader may refer to Hihara [9] to view individually plotted polarization diagrams containing the standard-deviation bars.

ZRA Experiments:

The galvanic current I_{GALV} and galvanic potential E_{GALV} were measured with a self-built ZRA and electrometer. Field-effect transistor (FET) operational amplifiers with high input impedance (10^{15} ohm) and low offset voltage (< 0.5 mV) (OPA 104 CM, Burr-Brown), and high-precision resistors (10^3 to 10^9 ohm, tolerance better than 2%) were used to build the ZRA. The electrometer was built with the OPA 104 CM operational amplifier. The circuitry can be obtained from Hihara [9]. Saturated Calomel or saturated mercury-mercurous sulfate reference electrodes were used to measure E_{GALV}. To prevent chloride contamination in 0.5 M Na_2SO_4 during lengthy experiments, the mercury-mercurous sulfate electrode was used instead of the Calomel electrode. Values of I_{GALV} and E_{GALV} were

measured from galvanic couples consisting of P100 G fibers and 6061-T6 Al of equal surface areas.

Results

To identify galvanic couples using the mixed-electrode theory, collections of cathodic polarization diagrams of P100 G, SiC, and TiB_2 were plotted with anodic polarization diagrams of m5N Al and 6061-T6 Al in Figure 1 (for deaerated 0.5 M Na_2SO_4), Figure 2 (for aerated 0.5 M Na_2SO_4), Figure 3 (for deaerated 3.15 wt% NaCl), and Figure 4 (for aerated 3.15 wt% NaCl). Compared in Figure 5 are the anodic polarization diagrams of the 0.0233 cm^2 and the 0.811 cm^2 6061-T6 Al electrodes exposed to 0.5 M Na_2SO_4.

The galvanic-corrosion rate i_{GALV} (Figure 6) and potential E_{GALV} (Figure 7) were monitored over 100-h periods for couples consisting of equal areas of P100 G fiber and 6061-T6 Al exposed to deaerated and aerated 0.5 M Na_2SO_4 and 3.15 wt% NaCl. The galvanic-corrosion rate i_{GALV} is normalized with respect to the 6061-T6 Al electrode area.

By using three different experimental methods (see Discussion), the galvanic-corrosion rate i_{GALV} was determined for galvanic couples consisting of equal areas of P100 G fiber and 6061-T6 Al. Results are tabulated in Table 1.

Discussion

Corrosion mechanisms of G-Al, SiC-Al, and TiB_2-Al galvanic couples are discussed in the first section. The second section compares galvanic-corrosion rates of G-Al couples that were determined using three different experimental methods. Finally, in the last section, Al corrosion rates are graphically

represented as functions of the area fraction of P100 G, SiC, and TiB_2.

Corrosion Mechanisms

The effect of deaeration, aeration, and chloride on galvanic-corrosion behavior was studied. Polarization behavior was examined in deaerated and aerated 0.5 M Na_2SO_4 and 3.15 wt% NaCl. The galvanic-corrosion rate of couples formed between Al (i.e., m5N Al and 6061-T6 Al) and the noble constituents (i.e., P100 G, SiC, and TiB_2) can be predicted by using the mixed-electrode theory. Cathodic polarization diagrams of the noble constituents were plotted together with the anodic polarization diagrams of m5N Al and 6061-T6 Al. The point of intersection between the cathodic and anodic curves gives the coordinates of the galvanic-corrosion rate i_{GALV} and potential E_{GALV}. Since the polarization curves are plotted as a function of CD, the galvanic-corrosion rate i_{GALV} and potential E_{GALV} will correspond to couples that have equal surface areas of Al and noble constituent.

Figure 1 shows the case for deaerated 0.5 M Na_2SO_4. The shapes of the cathodic polarization curves of the noble constituents are not very similar. The curve for TiB_2 is Tafel-like, whereas; the curves for P100G and SiC show a concentration-polarization-like regime followed by a Tafel-like regime. The Tafel-like behavior observed for TiB_2 and that which emerges at the higher CDs for SiC and P100G should be due to H^+ reduction. The anodic curves of m5N Al and 6061-T6 Al were similar and showed that the ultrapure metal and the alloy were passive. The passive CD was about 10^{-6} A/cm^2. One can predict using the mixed-electrode theory that the galvanic-corrosion rate should not exceed the passive Al CD.

Therefore, galvanic corrosion should be negligible in deaerated chloride-free environments.

There was a significant increase in the cathodic CDs of P100 G, SiC and TiB_2 in aerated 0.5 M Na_2SO_4 (Figure 2) as compared to deaerated 0.5 M Na_2SO_4 (Figure 1). The increase in cathodic CD was a result of O_2 reduction. Aeration did not have significant effects on the passivation of m5N Al and 6061-T6 Al, and therefore, the galvanic-corrosion rate should be similar to that in deaerated 0.5 M Na_2SO_4.

In deaerated 3.15 wt% NaCl (Figure 3), the cathodic curves of the noble constituents were similar to those in deaerated 0.5 M Na_2SO_4 (Figure 1). However, both m5N Al and 6061-T6 Al were susceptible to pitting at potentials greater than about -0.7 V_{SCE}. As shown in Figure 3, the cathodic curves of the noble constituents intersect the anodic curves of m5N Al and 6061-T6 Al in the passive regime (i.e., at potentials below the pitting potential). Therefore, the galvanic-corrosion rate is limited to the passive CD (about 10^{-6} A/cm^2).

In aerated 3.15 wt% NaCl (Figure 4), the cathodic curves of the noble constituents are similar to those in aerated 0.5 M Na_2SO_4 (Figure 2). The m5N Al and 6061-T6 Al pitted at potentials greater than about -0.7 V_{SCE}. The mixed-electrode theory indicates that the noble constituents will polarize m5N Al and 6061-T6 Al into the pitting regime. Galvanic-corrosion rates can be expected to be significant in aerated chloride-containing environments.

A few comments on the resistivity of SiC and its effect on galvanic corrosion are due. The resistivity of SiC can range from 10^{-5} to 10^{+13} ohm-cm depending on its purity [10]. When a

cathodic reaction occurs on an SiC particle of high resistivity, a large IR drop can develop by the flow of current through the particle. Galvanic-corrosion rates would be significantly reduced by a large IR drop. The IR drop through a particle is approximately equal to $i\rho l$, as a first approximation (Figure 8), where i is the cathodic CD through the particle, ρ is the resistivity of the particle, and l is roughly the size of the particle. In SiC/Al MMCs, very small SiC particles are used, and therefore, the IR drop could be insignificant. For example, an IR drop of only 4 mV would result from a 40 μm particle of 10^5 ohm-cm resistivity upon which O_2 reduction occurred at a rate of 10^{-5} A/cm^2. A 4 mV IR drop would essentially have no effect on galvanic corrosion.

Comparison of Galvanic-Corrosion Rates Determined by Different Experimental Methods

The galvanic-corrosion rate for a couple consisting of equal areas of P100 G and 6061-T6 Al was determined from three different methods for deaerated and aerated 0.5 M Na_2SO_4 and 3.15 wt% NaCl solutions. The galvanic-corrosion rates are tabulated in Table 1.

In the first method, i_{GALV} was read from polarization diagrams of P100 G and 6061-T6 Al in Figures 1 through 4 using the mixed-electrode theory. Values of i_{GALV} were also obtained from the ZRA technique. The values that are listed in Table 1 correspond to measurements taken at 100 hours from the curves in Figure 6. In the last method, i_{GALV} was derived from the corrosion rate i_{CORR} that was extrapolated from polarization diagrams (not shown) of a commercial G/6061-T6 Al MMC that contained 50 vol.% of fibers. The value of i_{GALV} is twice that of i_{CORR} because i_{GALV} is normalized with respect to the 6061-T6 Al

matrix area; whereas, i_{CORR} is normalized with respect to the composite area.

The values of i_{GALV}, determined from the three methods, were in good agreement for deaerated 0.5 M Na_2SO_4 and 3.15 wt% NaCl. All values (see Table 1) were within an order of magnitude of the 6061-T6 Al passive CD (about 10^{-6} A/cm^2). Excellent agreement among the three methods also prevailed for aerated 3.15 wt% NaCl. The corrosion rate ranged from 1×10^{-4} to 3×10^{-4} A/cm^2. See Table 1.

In aerated 0.5 M Na_2SO_4, the value of i_{GALV} from the ZRA technique was about 10 to 100 times greater than that from the mixed-electrode theory (about 10^{-6} A/cm^2). That discrepancy could have been caused by a change in the dissolution behavior of 6061-T6 Al over the duration of the ZRA experiment, and an edge effect of the 6061-T6 Al electrodes. During the ZRA experiment, i_{GALV} increased with time in two out of three experiments (Figure 6); whereas, E_{GALV} decreased with time (Figure 7). An increasing i_{GALV} accompanied by a decreasing E_{GALV} indicates that the anodic polarization curve of 6061-T6 Al shifted to the right (to larger CDs) on a log i-E diagram. In addition, the 6061-T6 Al electrodes used in the ZRA experiments had larger edge-to-surface area ratios than the electrodes used for the mixed-electrode theory. It is possible that large edge-to-surface area ratio is associated with high dissolution rates. Notice in Figure 5 that the anodic CD of 6061-T6 Al is about five times higher for the 0.0233 cm^2 electrodes that were used in the ZRA experiments compared to the 0.811 cm^2 electrodes that were used to generate the polarization diagrams for the mixed-electrode theory. The small

electrode has an edge-to-surface area ratio that is greater than that of the large electrode.

The value of i_{GALV} that was derived from the commercial G/6061-T6 Al MMC exposed to aerated 0.5 M Na_2SO_4 was not compared to i_{GALV} from the ZRA experiment or the mixed-electrode theory. The composite is contaminated with microstructural chloride that induces pitting of the 6061-T6 Al matrix in aerated 0.5 M Na_2SO_4 [11]; thus, the value of i_{GALV} does not truly correspond to that from an aerated chloride-free environment. In the previous cases (i.e. deaerated 0.5 M Na_2SO_4 and 3.15 wt% NaCl), however, the value of i_{GALV} derived from the commercial composite was considered valid for the following reasons. In deaerated 0.5 M Na_2SO_4, the 6061-T6 Al matrix was passive in the open-circuit condition (polarization diagram not shown), showing that microstructural chloride had negligible effects on corrosion behavior. In 3.15 wt% NaCl, the effects of microstructural chloride should not be pronounced because the solution contains high levels of chloride.

Graphical Representation of Galvanic-Corrosion Rates

Results have indicated that galvanic corrosion will be severe in aerated chloride-containing environments. Therefore, a graph (Figure 9) was generated from which the galvanic-corrosion rate of an m5N Al or 6061-T6 Al matrix can be obtained as a function the P100 G, SiC, or TiB_2 area fraction.

The mixed-electrode theory was used to develop the graph. In a galvanic couple, the current that flows from the cathode I_C is equal to the current that flows to the anode I_A. The subscripts "c" and "a" refer to cathode and anode, respectively,

and will also apply to other parameters. Both I_C and I_A are equivalent to the galvanic current I_{GALV}:

$$I_C = I_A = I_{GALV} \quad (1)$$

The cathodic and anodic currents can be written in terms of current density i and electrode area A:

$$I_C = i_C \bullet A_C \quad (2)$$

and

$$I_A = i_A \bullet A_A \quad (3).$$

Substituting (2) and (3) into (1), gives

$$i_C \bullet A_C = i_A \bullet A_A \quad (4).$$

Equation (4) can be written in terms of area fractions X_C and X_A, by dividing both sides of (4) by $A_C + A_A$:

$$i_C \bullet X_C = i_A \bullet X_A \quad (5)$$

Since $X_C + X_A = 1$, Equation (5) can be simplified to

$$i_A = i_C \bullet (X_C / 1\text{-}X_C) \quad (6).$$

The parameter i_A (the dissolution rate of the anode) is the galvanic-corrosion rate i_{GALV}.

When the value of i_C is known, equation 6 shows that i_{GALV} can be plotted as a function of the cathode area fraction X_C to generate the X_C-log i_{GALV} plot in Figure 9. Examination of Figure 4 shows that the value of i_C should be equal to the CD of the cathodic constituents in the pitting regime of m5N Al and 6061-T6 Al. Read from Figure 4, the value of i_C for P100 G is

about 3.2×10^{-4} A/cm^2, and about 1.0×10^{-5} A/cm^2 for SiC and TiB_2. Since the anodic polarization curves of m5N Al and 6061-T6 Al are almost identical in the pitting regime, the ultrapure metal and alloy should have similar galvanic-corrosion behavior. Thus, it will not be advantageous to use m5N Al in place of 6061-T6 Al for the purpose of improving resistance to galvanic corrosion. There is an exception, however, when X_C is small. This is demonstrated in Figure 10, which shows that for a critical value of X_C less than 0.003, the cathodic P100 G curve intersects the anodic m5N Al curve in the passive regime. Note that there is no passive regime for 6061-T6 Al; thus, the galvanic-corrosion behavior of m5N Al and 6061-T6 deviates at X_C less than 0.003. For SiC and TiB_2, the critical value of X_C is 0.08. Also note that cathodic partial reactions occurring on the anode cannot be accounted for; thus, the true dissolution rate of the matrix is greater than the value of i_{GALV}.

The X_C-log i_{GALV} plot in Figure 9 shows that i_{GALV} is about 30 times greater for G-Al couples compared to SiC-Al couples. The graphs also show that i_{GALV} of 6061-T6 Al coupled to an equal area of P100 G is about 80 times the corrosion rate of uncoupled 6061-T6 Al. In contrast, i_{GALV} of 6061-T6 Al coupled to SiC or TiB_2 is only about 2.5 times the corrosion rate of the uncoupled alloy. Thus, the corrosion resistance of SiC/Al MMCs should be significantly greater than that of G/Al MMCs.

Conclusions

Galvanic corrosion of G/Al and SiC/Al MMCs can be expected to be significant in aerated chloride-containing environments. Experiments have shown that the corrosion rate was controlled by the rate of O_2 reduction, which was significantly greater on P100 G than on SiC. Therefore, G/Al

MMCs should corrode many times faster than SiC/Al MMCs. Results also indicate that resistance to galvanic corrosion cannot be improved by using m5N Al for matrix material in place of 6061-T6 Al. In the absence of dissolved O_2, galvanic corrosion should be negligible.

Acknowledgements

We are grateful for the financial support provided by the Shell Companies Foundation and the Office of Naval Research (grant # N00014-89-J-1588). We are particularly grateful to Dr. A.J. Sedriks of the Office of Naval Research.

References

1) M. Pourbaix, Atlas of Electrochemical Equilibria in Aqueous Solutions, National Association of Corrosion Engineers, 1974.

2) E.G. Kendall, D.L. Dull, "Salt Water Corrosion Behavior of Aluminum-Graphite Composite," National Technical Information Service, U.S. Department of Commerce, AD-777 160, 1974.

3) D.L. Dull, W.C. Harrigan, Jr., M.F. Amateau, Aerospace Corporation, AD - A011 761, 1975.

4) W.H. Pfeifer, in Hybrid and Select Metal-Matrix Composites, Ed. W.J. Renton, American Institute of Aeronautics and Astronautics, 1977, p.231.

5) D.M. Aylor, R.M. Kain, in Recent Advances in Composites in the United States and Japan, Ed. J.R. Vinson, M. Taya, ASTM Special Technical Publication 864, 1983, p.632.

6) M.G. Vassilaros, D.A. Davis, G.L. Steckel, J.P. Gudas, in Mechanical Behavior of Metal-Matrix Composites, Ed. J.E. Hack, M.F. Amateau, The Metallurgical Society of the AIME, 1983, p.335.

7) W.F. Czyrklis, Corrosion/85, Paper No. 196, National Association of Corrosion Engineers, Houston, Texas, 1985.

8) K.D. Lore, J.S. Wolf, Extended Abstracts, Vol. 81-2, The Electrochemical Society, Denver, Colorado, 1981, p.387.

9) L.H. Hihara, "Corrosion of Aluminum-Matrix Composites," Ph.D. Thesis, Massachusetts Institute of Technology, 1989.

10) N. Ichinose, Ed., Introduction to Fine Ceramics, John Wiley and Sons Ltd., 1987, p. 52.

11) L.H. Hihara, R.M. Latanision, Corrosion, in press.

List of Figures

Figure 1: A collection of polarization diagrams for calculation of galvanic-corrosion rates using the mixed-electrode theory. Deaerated 0.5 M Na_2SO_4 of pH 7 at 30°C. Scan rate = 0.1 mV/s.

Figure 2: A collection of polarization diagrams generated in aerated 0.5 M Na_2SO_4 of pH 7 at 30°C. Scan rate = 0.1 mV/s.

Figure 3: A collection of polarization diagrams generated in deaerated 3.15 wt% NaCl of pH 7 at 30°C. Scan rate = 0.1 mV/s.

Figure 4: A collection of polarization diagrams generated in aerated 3.15 wt% NaCl of pH 7 at 30°C. Scan rate = 0.1 mV/s.

Figure 5: Anodic polarization diagrams of 6061-T6 Al electrodes of two different sizes. The anodic CDs of the 0.0233 cm^2 electrode are about five times greater than that of the 0.811 cm^2 electrode. Aerated 0.5 M Na_2SO_4 of pH 7 at 30°C. Scan rate = 0.1 mV/s.

Figure 6: Galvanic-corrosion rate i_{GALV} of galvanic couples consisting of P100 G and 6061-T6 Al of equal areas exposed to neutral solutions at 30°C.

Figure 7: Galvanic-corrosion potentials E_{GALV} of couples consisting of P100 G and 6061-T6 Al of equal areas exposed to neutral solutions at 30°C.

Figure 8: A first approximation of the IR drop through an SiC particle, assuming one-dimensional current flow through the particle. $I = il^2$, $R = \rho l/l^2$, $IR = i\rho l$.

Figure 9: Graphs showing the galvanic-corrosion rate i_{GALV} of m5N Al and 6061-T6 Al as a function of area fraction X_C of P100 G, SiC, and TiB_2 in aerated 3.15 wt% NaCl of pH 7 at 30°C.

Figure 10: A collection of polarization diagrams to show the effect of P100 G area fraction X_C on galvanic-corrosion behavior in aerated 3.15 wt% NaCl of pH 7 at 30°C. Note that galvanic-corrosion behavior of m5N Al and 6061-T6 Al deviates for X_C less than 0.003 due to passivation of m5N Al. Polarization currents are based on the given areas.

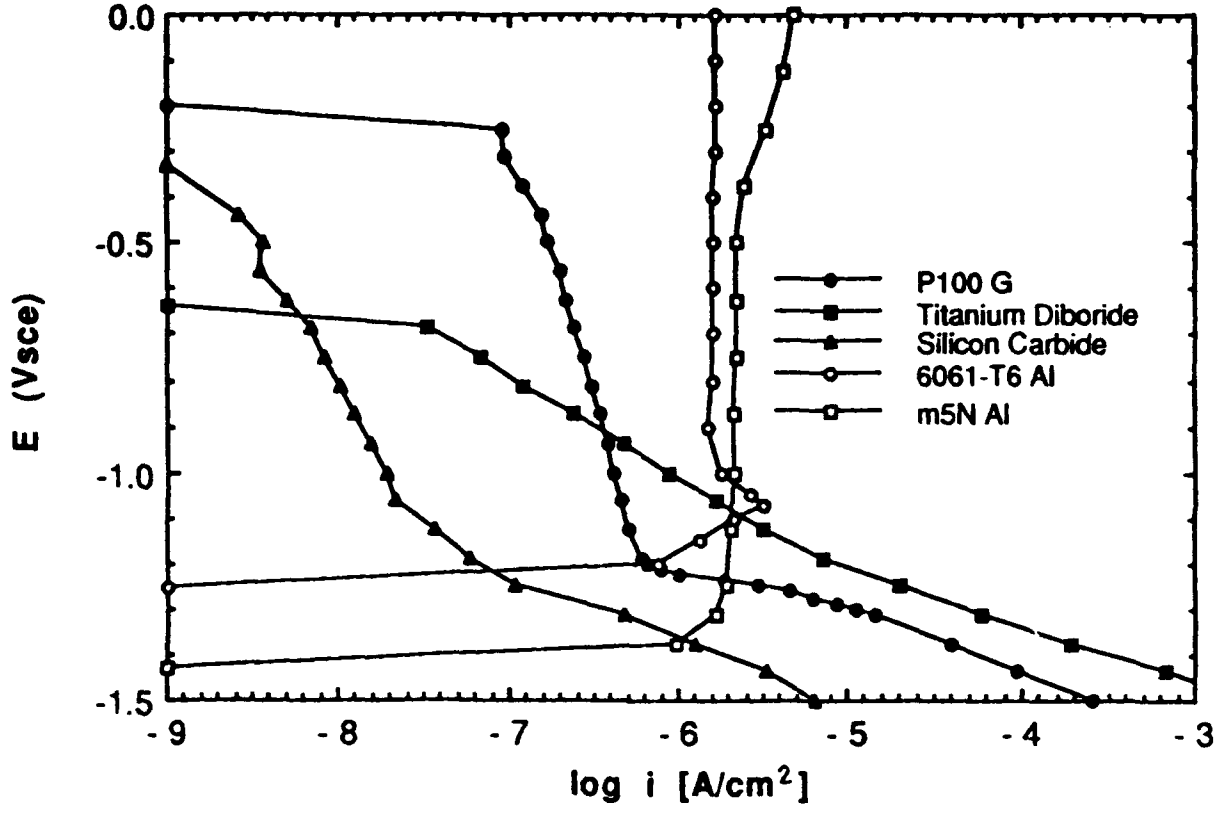

Figure 1: A collection of polarization diagrams for calculation of galvanic-corrosion rates using the mixed-electrode theory. Deaerated 0.5 M Na_2SO_4 of pH 7 at 30°C. Scan rate = 0.1 mV/s.

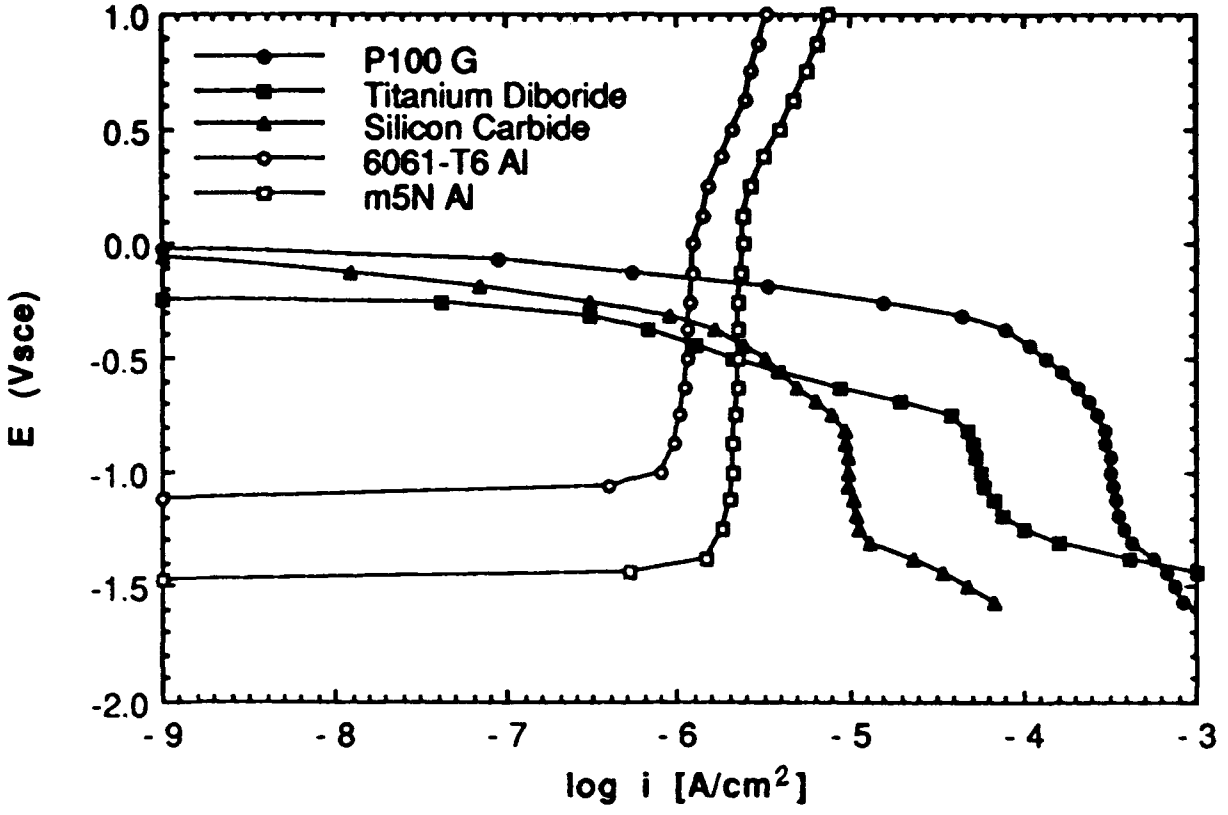

Figure 2: A collection of polarization diagrams generated in aerated 0.5 M Na_2SO_4 of pH 7 at 30°C. Scan rate = 0.1 mV/s.

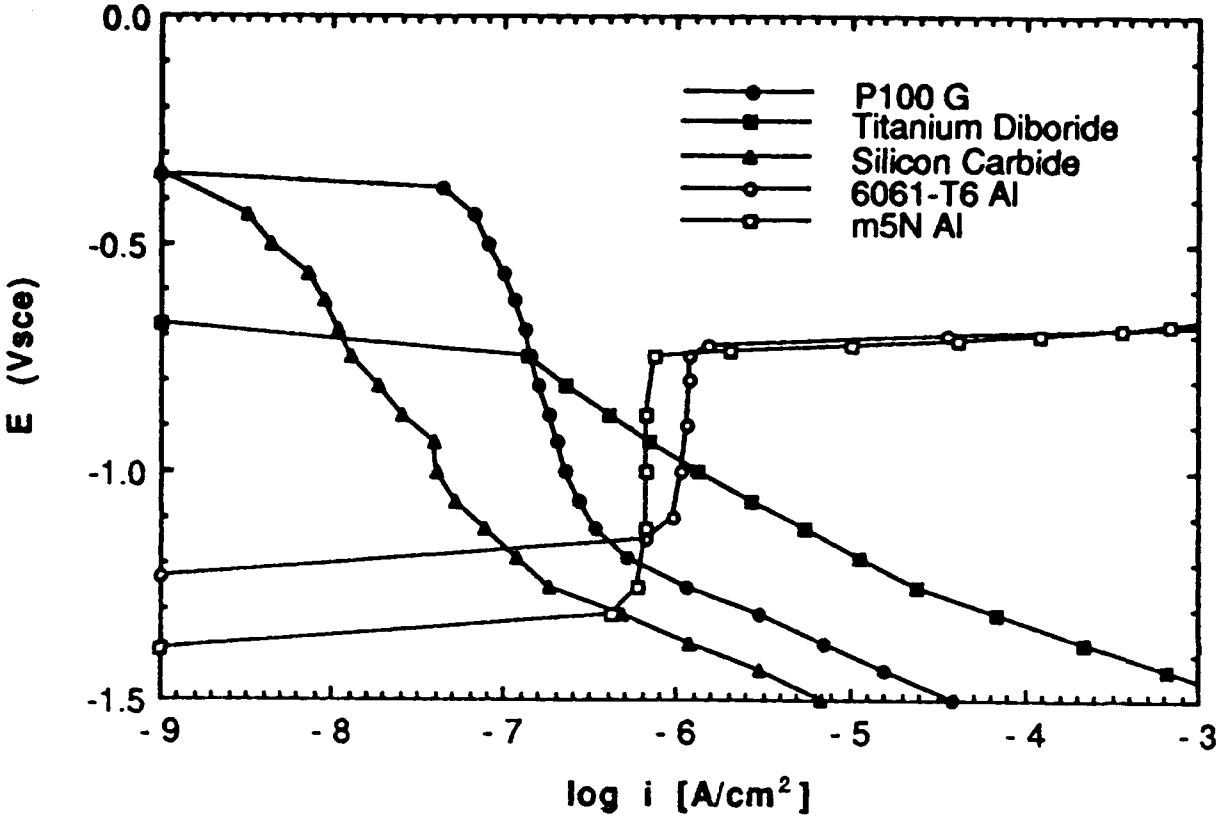

Figure 3: A collection of polarization diagrams generated in deaerated 3.15 wt% NaCl of pH 7 at 30°C. Scan rate = 0.1 mV/s.

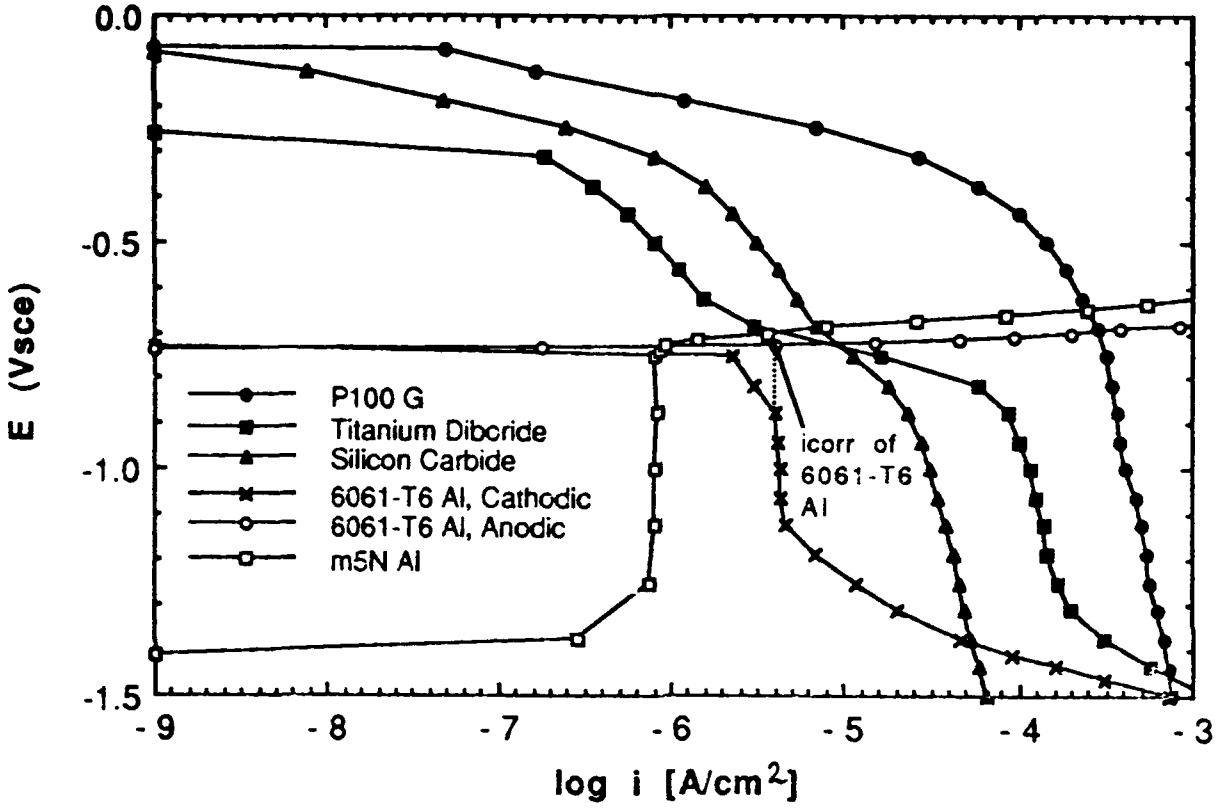

Figure 4: A collection of polarization diagrams generated in aerated 3.15 wt% NaCl of pH 7 at 30°C. Scan rate = 0.1 mV/s.

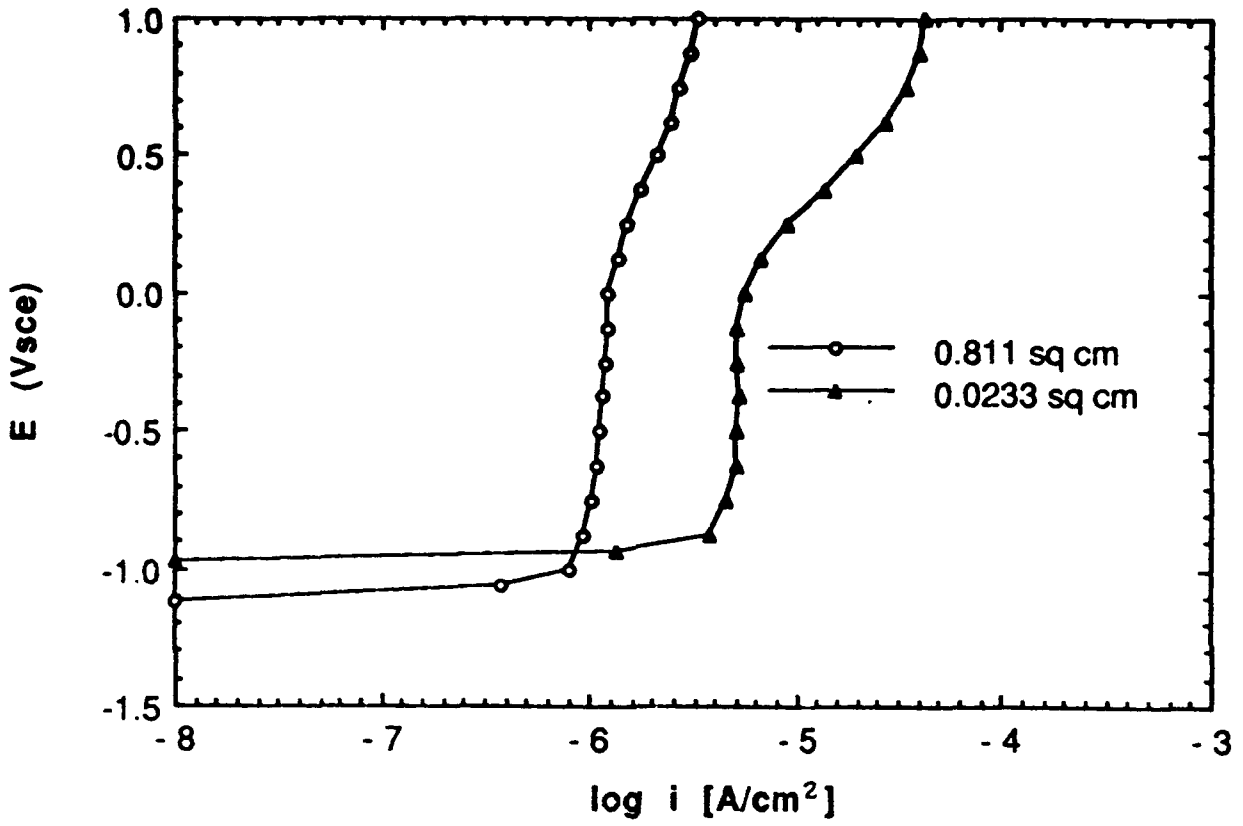

Figure 5: Anodic polarization diagrams of 6061-T6 Al electrodes of two different sizes. The anodic CDs of the 0.0233 cm^2 electrode are about five times greater than that of the 0.811 cm^2 electrode. Aerated 0.5 M Na_2SO_4 of pH 7 at 30°C. Scan rate = 0.1 mV/s.

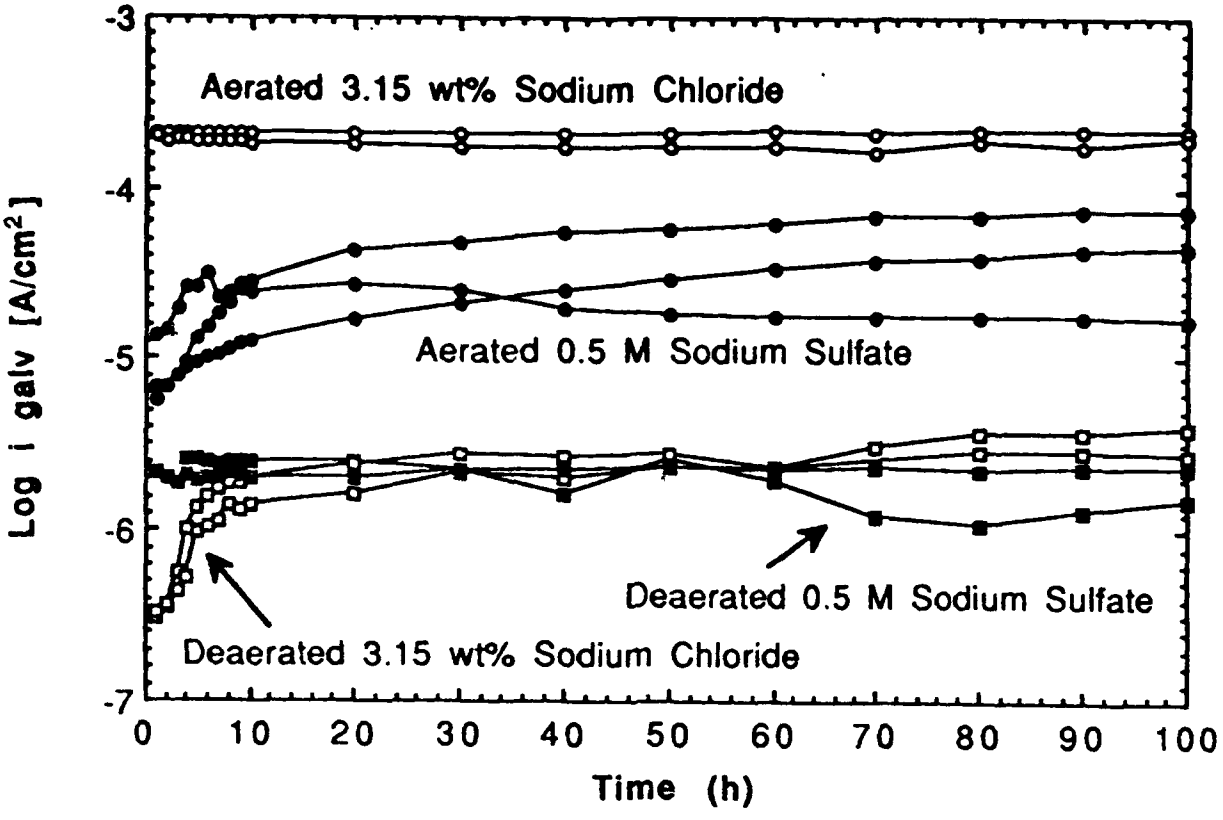

Figure 6: Galvanic-corrosion rate i_{GALV} of galvanic couples consisting of P100 G and 6061-T6 Al of equal areas exposed to neutral solutions at 30°C.

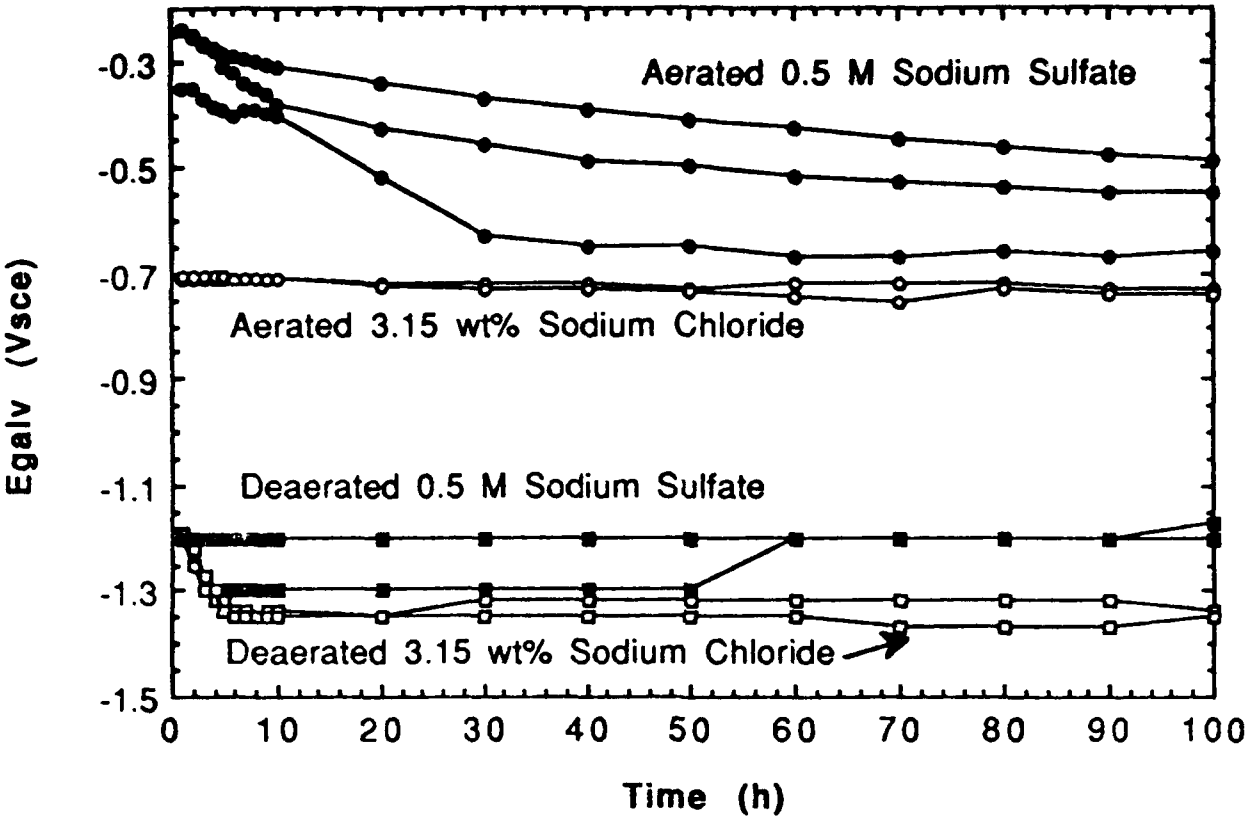

Figure 7: Galvanic-corrosion potentials E_{GALV} of couples consisting of P100 G and 6061-T6 Al of equal areas exposed to neutral solutions at 30°C.

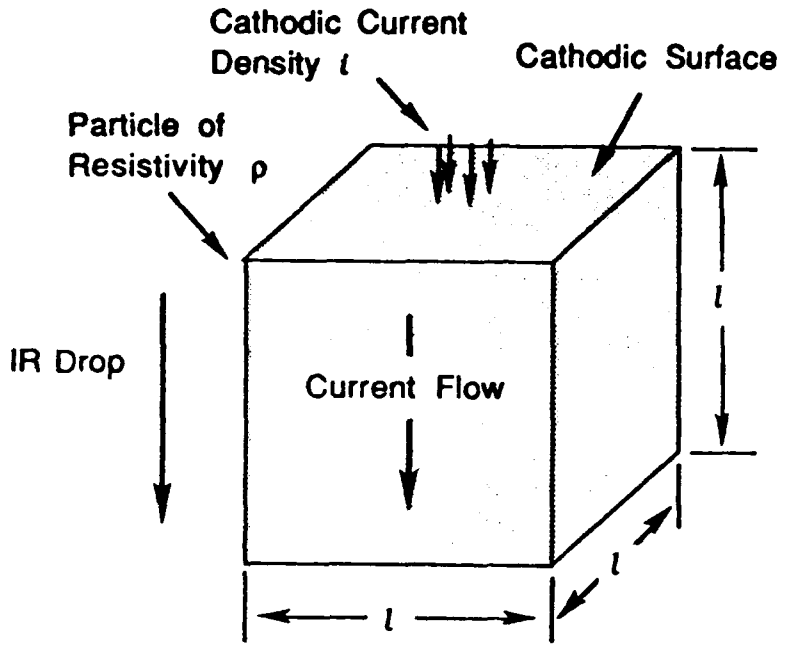

Figure 8: A first approximation of the IR drop through an SiC particle, assuming one-dimensional current flow through the particle. $I = il^2$, $R = \rho l/l^2$, $IR = i\rho l$.

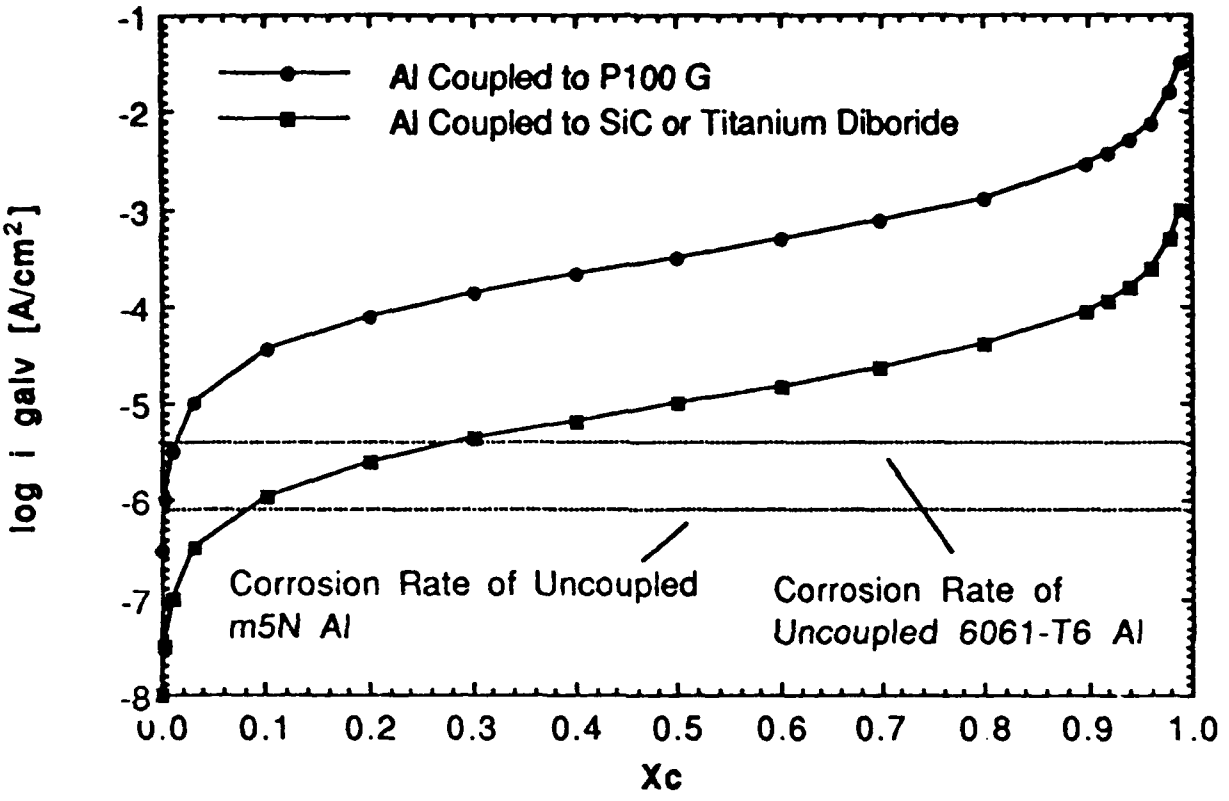

Figure 9: Graphs showing the galvanic-corrosion rate i_{GALV} of m5N Al and 6061-T6 Al as a function of area fraction X_C of P100 G, SiC, and TiB_2 in aerated 3.15 wt% NaCl of pH 7 at 30°C.

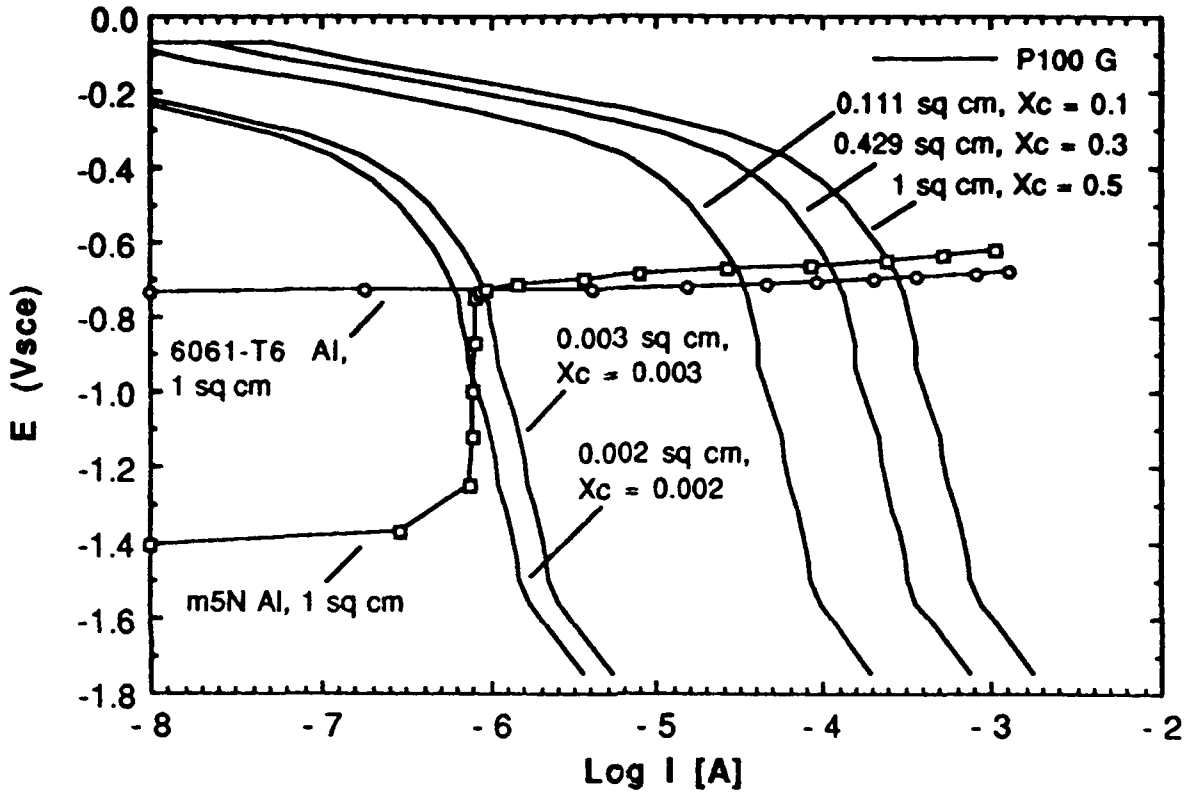

Figure 10: A collection of polarization diagrams to show the effect of P100 G area fraction X_c on galvanic-corrosion behavior in aerated 3.15 wt% NaCl of pH 7 at 30°C. Note that galvanic-corrosion behavior of m5N Al and 6061-T6 Al deviates for X_c less than 0.003 due to passivation of m5N Al. Polarization currents are based on the given areas.

RE/1131/88/75
4315 (036)

Supplemental Distribution List — Feb 1990

Profs. G.H. Meier and F.S.Pettit
Dept. of Metallurgical and
Materials Eng.
University of Pittsburgh
Pittsburgh, PA 15261

Prof. H.K. Birnbaum
Dept. of Metallurgy & Mining Eng.
University of Illinois
Urbana, Ill 61801

Prof. H.W. Pickering
Dept. of Materials Science and Eng.
The Pennsylvania State University
University Park, PA 16802

Prof. D.J. Duquette
Dept. of Metallurgical Eng.
Rensselaer Polytechnic Inst.
Troy, NY 12181

Prof. D. Tomanek
Michigan State University
Dept. of Physics and Astronomy
East Lansing, MI 48824-1116

Dr. M. W. Kendig
Rockwell International Science Center
1049 Camino Dos Rios
P.O. Box 1085
Thousand Oaks, CA 91360

Prof. R. A. Rapp
Dept. of Metallurgical Eng.
The Ohio State University
116 West 19th Avenue
Columbus, OH 43210-1179

Dr. R. W. Drisko
Code L-52
Naval Civil Engineering Laboratory
Port Hueneme, CA 93043-5003

Dr. R.D. Granata
Zettlemoyer Center for Surface Studies
Sinclair Laboratory, Bld. No. 7
Lehigh University
Bethlehem, PA 18015

Dr. G. D. Davis
Martin Marietta Laboratories
1450 South Rolling Rd.
Baltimore, MD 21227-3898

Prof. P.J. Moran
Dept. of Materials Science & Eng.
The Johns Hopkins University
Baltimore, MD 21218

Prof. J. Kruger
Dept. of Materials Science & Eng.
The Johns Hopkins University
Baltimore, MD 21218

Dr. B.G. Pound
SRI International
333 Ravenswood Ave.
Menlo Park, CA 94025

Prof. C.R. Clayton
Department of Materials Science
& Engineering
State University of New York
Stony Brook
Long Island, NY 11794

Dr. J. W. Oldfield
Cortest Laboratories Ltd
23 Shepherd Street
Sheffield, S3 7BA, England

Prof. Boris D. Cahan
Dept. of Chemistry
Case Western Reserve Univ.
Cleveland, Ohio 44106

Prof. G. Simkovich
Dept. of Materials Science & Eng.
The Pennsylvania State University
University Park, PA 16802

Prof. M.E. Orazem
Dept. of Chemical Engineering
University of Florida
Gainesville, FL 32611

Dr. P. S. Pao
Code 6303
Naval Research Laboratory
Washington, D.C. 20375

Dr. N. S. Bornstein
United Technologies Research Center
East Hartford, CT 06108

Prof. R. M. Latanision
Massachusetts Institute of Technology
Room 8-202
Cambridge, MA 02139

Dr. R. E. Ricker
National Institute of Standards and Technology
Metallurgy Division
Bldg. 223, Room B-266
Gaithersburg, MD 20899

Dr. F. B. Mansfeld
Dept. of Materials Science
University of Southern California
University Park
Los Angeles, CA 90089

Dr. W. R. Bitler
Dept. of Materials Sci. and Eng.
115 Steidle Building
The Pennsylvania State University
University Park, PA 16802

Dr. S. Smialowska
Dept. of Metallurgical Engineering
The Ohio State University
116 West 19th Avenue
Columbus, OH 43210-1179

Dr. R. V. Sara
Union Carbide Corporation
UCAR Carbon Company Inc.
Parma Technical Center
12900 Snow Road
Parma, Ohio 44130

Prof. G.R. St. Pierre
Dept. of Metallurgical Eng.
The Ohio State University
116 West 19th Avenue
Columbus, Oh 43210-1179

Dr. E. McCafferty
Code 6322
Naval Research Laboratory
Washington, D. C. 20375

Prof. J. O'M. Bockris
Dept. of Chemistry
Texas A & M University
College Station, TX 77843

Dr. V. S. Agarwala
Code 6062
Naval Air Development Center
Warminster, PA 18974-5000

Prof. Harovel G. Wheat
Dept. of Mechanical Engineering
The University of Texas
ETC 11 5.160
Austin, TX 78712-1063

Prof. S. C. Dexter
College of Marine Studies
University of Delaware
700 Pilottown Rd.
Lewes, DE 19958

BASIC DISTRIBUTION LIST

Technical Reports and Publications **Feb 1990**

Organization	Copies
Defense Documentation Center Cameron Station Alexandria, VA 22314	12
Office of Naval Research Dept. of the Navy 800 N. Quincy Street Arlington, VA 22217 ATTN: Code 1131	3
Naval Research Laboratory Washington, DC 20375 ATTN: Codes 6000	1
6300	1
2627	1
Naval Air Development Center Code 606 Warminster, PA 18974 ATTN: Dr. J. DeLuccia	1
Commanding Officer Naval Surface Warfare Center Silver Spring, MD 20903-5000 ATTN: Library	1
Code R33	1
Naval Ocean Systems Center San Diego, CA 92152-5000 ATTN: Library	1
Naval Postgraduate School Monterey, CA 93940 ATTN: Mechanical Engineering Department	1
Naval Air Systems Command Washington, DC 20360 ATTN: Code 310A	1
Code 5304B	1
Code 931A	1
Naval Sea Systems Command Washington, DC 20362 ATTN: Code 05M	1
Code 05R	1

Organization	Copies
Naval Air Propulsion Center Trenton, NJ 08628 ATTN: Library	1
Naval Civil Engineering Laboratory Port Hueneme, CA 94043 ATTN: Materials Div.	1
Naval Electronics Laboratory San Diego, CA 92152 ATTN: Electronic Materials Sciences Division	1
Commander David Taylor Research Center Bethesda, MD 20084	1
Naval Underwater System Ctr. Newport, RI 02840 ATTN: Library	1
Naval Weapons Center China Lake, CA 93555 ATTN: Library	1
NASA Lewis Research Center 21000 Brookpark Road Cleveland, OH 44135 ATTN: Library	1
National Institute of Standards and Technology Gaithersburg, MD 20899 ATTN: Metallurgy Division	1
Ceramics Division	1
Fracture & Deformation Division	1

Naval Facilities Engineering
Command
Alexandria, VA 22331
ATTN: Code 03 1

Commandant of the Marine Corps 1
Scientific Advisor
Washington, DC 20380
ATTN: Code AX 1

Army Research Office
P.O. Box 12211
Research Triangle Park, NC 27709
ATTN: Metallurgy & Ceramics
Program 1

Army Materials Technology Laboratory
Watertown, MA 02172-0001
ATTN: Research Program Office 1

Air Force Office of Scientific
Research
Building 410
Bolling Air Force Base
Washington, DC 20332
ATTN: Electronics & Materials
Science Directorate 1

NASA Headquarters
Washington, DC 20546
ATTN: Code RM 1

Defense Metals & Ceramics
Information Center
Battelle Memorial Inst.
505 King Avenue
Columbus, OH 43201 1

Oak Ridge National Laboratory
Metals and Ceramics Div.
P.O. Box X
Oak Ridge, TN 37380 1
Oak Ridge, TN 37380 1

Los Alamos Scientific Lab.
P.O. Box 1663
Los Alamos, NM 87544
ATTN: Report Librarian 1

Argonne National Laboratory
Metallurgy Division
P.O. Box 229
Lemont, IL 60439 1

Brookhaven National Laboratory
Technical Information Division
Upton, Long Island
New York 11973
ATTN: Research Library 1

Lawrence Berkeley Lab.
1 Cyclotron Rd
Berkeley, CA 94720
ATTN: Library 1

David Taylor Research Ctr
Annapolis, MD 21402-5067
ATTN: Code 281 1
Code 2813 1
Code 0115 1